The coupling of a synthetic turbulence generator with turbomachinery boundary conditions

S. Leyh and C. Morsbach

1 Introduction

The power of modern computers and massive parallelization on clusters makes it possible to do scale-resolving simulations at *Reynolds* numbers relevant for turbomachinery. Since the computational domain can only represent a finite part of the physical world, it is essential for numerical simulation codes to provide high quality boundary conditions (BC) in the sense of non-reflective properties and the possibility of unsteady inflow.

If the inlet of the considered configuration is located in a turbulent region, the solver has to feature an appropriate boundary treatment. Especially in turbomachinery, the flow has a highly unsteady and turbulent character. Hence, the inlet boundary has to deal with both wakes of previous stages and turbulence. Since precursor simulations are very expensive and impractical for industrial configurations, there are numerous approaches of creating artificial (synthetic) turbulence. Popular examples are the Digital Filter Method [4], the Synthetic Eddy Method [3] and spectral methods based on the superposition of *Fourier* modes [5].

The latter method has been implemented into DLR's in-house turbomachinery code TRACE [8] and tested in combination with a source term formulation and a BC formulation [7]. Since TRACE provides a number of different boundary conditions, the present paper investigates the interaction of selected BCs with the turbulence generator.

S. Leyh · C. Morsbach
German Aerospace Center (DLR), Linder Höhe, Cologne, Germany, e-mail: `{sascha.leyh, christian.morsbach}@dlr.de`

2 Synthetic turbulence generator

The synthetic turbulence generator (STG) used in TRACE is described by Shur et al. [15] and was implemented by Morsbach and Franke [8] who adapted it for periodic domains. The turbulence dissipation rate ε in the original formulation is unknown and can be written as $\varepsilon = \beta k \omega$ [17, Eq. A4b]. With the turbulent length scale $L_T = \sqrt{k}/\omega$ [17, Eq. 24] the dissipation rate can be replaced by:

$$\varepsilon = \frac{\beta k^{\frac{3}{2}}}{L_T} \tag{1}$$

For the present work, the length scale L_T and the *Reynolds* stress tensor are prescribed. To calculate the *Reynolds* stresses of isotropic turbulence from a given turbulence intensity Tu, the initialized velocity as a result of the prescribed *Mach* number Ma, total temperature T_0 and the isentropic relation, as well as $a = \sqrt{\gamma R_s T}$ is used and assumed constant during the simulation.

3 Boundary conditions

In the finite-volume solver of TRACE, the BCs determine a set of primitive variables according to the respective theory, located at the face of the boundary cell. The used ghost cells are filled by an extrapolation polynomial of order zero or one. Furthermore, the inner cells are updated first and subsequently the BCs are evaluated with the new cell values.

The considered ***Dirichlet*** BC prescribes the velocity components and the static temperature. The velocity consists of a constant given mean part with superposed perturbations of the STG. The static pressure of the first inner cell and the given static temperature are used to calculate the density (ideal gas). The ghost cells are filled by linear extrapolation using the state of the first inner cell and the face state.

The BC of Sandhu and Sandham [11] is called **integrated characteristic** in this work and is based on the characteristic concept described by Thompson [16]. The basic equation is given as [11, Eq. 3.1]:

$$\mathbf{q} = \mathbf{q}_0 + \int \left(\frac{\partial \hat{F}}{\partial x}\right)_{\lambda_1} dt \quad , \quad \left(\frac{\partial \hat{F}}{\partial x}\right)_{\lambda_1} = \begin{pmatrix} \frac{1}{2a^2} \\ \frac{u}{2a^2} - \frac{1}{2a} \\ \frac{v}{2a^2} \\ \frac{w}{2a^2} \\ \frac{1}{2}\left|\mathbf{v}\right|^2 \frac{1}{2a^2} - \frac{u}{2a} + \frac{1}{2}\frac{1}{\gamma-1} \end{pmatrix} \mathscr{L}_1 \tag{2}$$

According to the authors, $\mathbf{q}_0$ in Eq. (2) "represents the forced basic flow behavior at the inflow boundary" [11, p. 6] and the integral is a "correction made to the inflow boundary [so that] the characteristic velocity λ_1 leaves the computational domain smoothly". $\frac{\partial \hat{F}}{\partial x}$ is the *Euler* part x-component of the conservation equations and is determined by a characteristic analysis of the 1D *Euler* equations. The outgoing wave amplitude $\mathscr{L}_1$ can be found in Poinsot and Lele [10, Eq. 19]. The integral in Eq. (2) is approximated with the same time scheme as used in the interior domain. Therefore the integrand is calculated with inner cell values before the time step update of the interior cells. Unlike the other BCs in this paper the resulting values are directly written into the ghost cells. Treating them as face values and filling the ghost cells by extrapolating leads to unstable behavior.

The ***Riemann*** BC is described e.g. by Carlson [1, p. 7] and is implemented with changed sequence. The total pressure and temperature, as well as the flow angle are given at the inflow. The outgoing *Riemann* invariant $j_- = u - \frac{2a}{\gamma-1}$ [1, Eq. 12] is calculated with values of the first inner cell and is extrapolated to the boundary face. Instead of assuming adiabatic flow, the total enthalpy h_t is calculated from the given total temperature. The difference of the invariants can be written as:

$$j_+ - j_- = \frac{4}{\gamma - 1} a \,, \tag{3}$$

and since the sonic speed a is a function of total enthalpy and the outgoing invariant, the incoming invariant $j_+ = u + \frac{2a}{\gamma-1}$ can be written as:

$$j_+ = \left(1 - \frac{4}{\gamma - 1}\right) j_- \pm \frac{4}{\gamma + 1} \sqrt{(\gamma + 1)\, h_t - \frac{\gamma - 1}{2} j_-^2} \,. \tag{4}$$

“The physically consistent result is the larger of the two roots” [1, p. 8]. With known values of both invariants the *Mach* number Ma and the sonic speed a are calculated. The velocity components are determined from the given inflow direction. The static pressure is calculated with the given total pressure and the known *Mach* number using the isentropic relation. This static pressure and the known sonic speed are used to calculate the density $\rho = \frac{\gamma p}{a^2}$. Since the turbulent perturbations are added to the calculated face state, the effective total pressure is larger than the prescribed value. Therefore, the total pressure has to be corrected for the turbulent kinetic energy.

The BC called **unsteady 1D characteristics** is described by Giles [2] and was implemented in TRACE by Schlüß et al. [13]. In this BC the eigenvector matrices L_{1D} [13, Eq. 20] and its inverse R_{1D} [13, Eq. 22] are used to transform primitive into characteristic variables and vice versa. The flow at the boundary is decomposed into three parts. The first part is a mean part designed to match the specified mean flow values using relaxation and a residual vector [13, Eq. 29]. A second part contains the instantaneous difference of the area-time averaged and area-averaged values. After transforming this primitive vector of perturbations into characteristic variables, the incoming characteristics are set to zero to obtain a non-reflective behavior. Another part consists of the difference of area-averaged and current values of the first inner cell and the incoming characteristic values are set to zero. Following the transformation of all parts into primitive variables, the STG output is added and the ghost cells are filled by linear extrapolation. As for the *Riemann* BC, the total pressure has to be corrected.

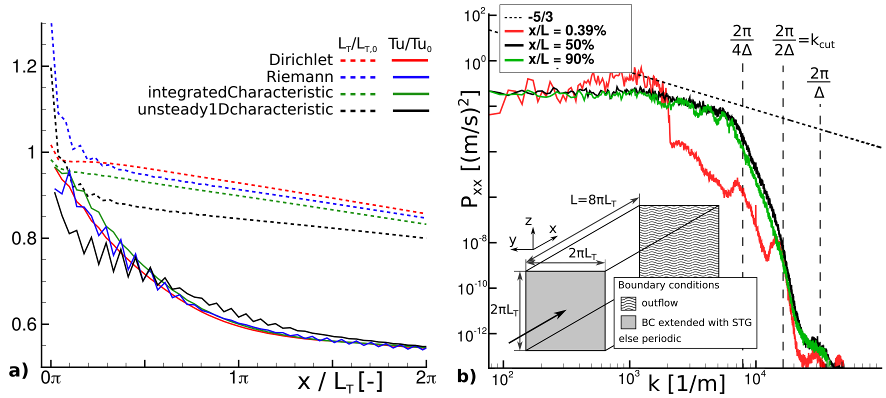

Fig. 1 a) Turbulent length scale and turbulence intensity for all considered BCs, b) Turbulence spectra for three streamwise positions

4 Test cases

To evaluate the basic properties of the coupled BCs, one of the two test cases is **homogeneous isotropic turbulence** in a cuboid domain. For given total pressure of $p_0 = 323555.53\ Pa$, total temperature of $T_0 = 300.9\ K$ and *Mach* number $Ma = 0.1$, the flow field is initialized with the static values of pressure and temperature. The velocity vector has only one non-zero component in x-direction with $u = Ma\sqrt{\gamma RT}$. The simulated time is prescribed by multiples of the throughflow time as ratio of domain size and mean velocity. To avoid averaging over the initial transient phase, recording statistics is started after 30 throughflows. The used subgrid-scale model is the Smagorinsky [14] model and the grid has $128 \times 32 \times 32$ points.

The second case is the **low-pressure-turbine profile T106C** designed by *MTU Aero Engines*. The simulation restarts from a RANS solution and uses a 3^{rd} order explicit *Runge-Kutta* scheme and the WALE subgrid-scale model [6]. The throughflow time is determined with a stream trace including the point of smallest distance of two adjacent blade surfaces and evaluating the needed time to pass the line part between the x-coordinates of the leading- and trailing edge. Using 0.005% of this time as time step, 20 throughflows are used to record statistics after 10 throughflows of transient phase. The span is equivalent to 40% of the chord length.

5 Results

The turbulence intensity Tu and length scale L_T, normalized with their respective prescribed values are presented in Fig. 1a). The *Dirichlet* and integrated characteristic BC reach a value near one ($x/L_T = 0$). A certain development length is apparent for the *Riemann* BC until the turbulence intensity distribution is located between the *Dirichlet* and integrated characteristic line. The differences obtained with the unsteady 1D characteristics BC can be explained by a too small normal component of the *Reynolds* stress in x-direction (not displayed). In general, the decay rates are similar. Hence, in Fig. 1b) only spectra for the *Dirichlet* BC are shown. In the first cell ($x/L = 0.39\%$) the spectrum has an undeveloped shape, but further downstream, the spectrum has a distinct section parallel to the dashed $-5/3$ line. Near the outlet, the spectrum shows oscillations in the $-5/3$ region, since the turbulence does not pass the outlet boundary cleanly. Furthermore, three wavenumbers associated with the edge length Δ of the cubic cells are marked. It can be seen, that wavelengths smaller than four cell sizes are strongly damped. These qualitative results are obtained with all tested BCs.

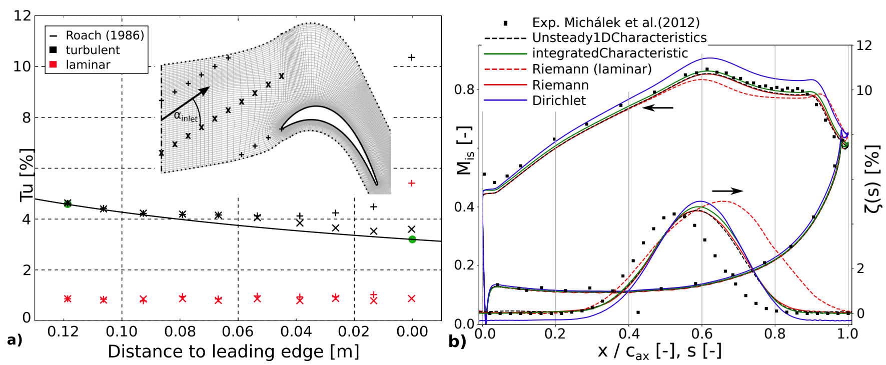

Fig. 2 T106C, $Tu = 0.032$, $L_T = 12\ mm$ a) Probe position and turbulence intensity for a laminar and turbulent simulation with the *Riemann* BC, b) Isentropic *Mach* number (left axis) and total pressure loss (right axis) for various BCs

To meet the given experimental inflow values of the T106C profile, the decay law by Roach [12] is used, as done by Michálek et al. [9]. In this way the value at the inlet can be reconstructed. In Fig. 2a), the simulation results show that the turbulence intensity at a line shifted by half of the pitch reaches a value near the target one (green circle). The turbulence intensity of nearly 1% for laminar inflow shows the effect of upstream traveling acoustic waves, produced by the wake flow. These waves are the reason why the isentropic *Mach* number in Fig. 2b) of the reflective *Dirichlet* simulation differs from all other BCs. Furthermore, with exception of the *Dirichlet* BC, the general level of the total pressure loss matches the exp. data provided by Michálek et al. [9], although the location of the wake does not coincide.

6 Conclusions

The STG has been coupled with four BCs. The results show a good agreement with the prescribed values of turbulent intensity and turbulent length scale. The simulation of homogeneous isotropic turbulence in a cuboid domain shows a physical spectrum downstream a certain development length. The analysis of a turbine profile isentropic *Mach* number distribution proves the importance of turbulent inflow conditions, since otherwise no meaningful results are obtained. Particularly for the pressure loss distribution, large discrepancies are obtained if the inflow is approximated as laminar. A next step could be the injection of non-isotropic turbulence and the specification of non-homogeneous input distributions.

References

1. Carlson, J-R.: Inflow/outflow boundary conditions with application to FUN3D, *Tech. Rep. NASA TM-2011-217181, NASA Langley Research Center*, (2011).
2. Giles, M.: UNSFLO: A numerical method for the calculation of unsteady flow in turobmachinery, *Tech. rep., Gas Turb. Lab. Report GTL 205, MIT Dept. of Aero. and Astro.*, (1991).
3. Jarrin, N., Benhamadouche, S., Laurence, D., and Prosser, R.: A synthetic-eddy-method for generating inflow conditions for large-eddy simulations, *Int. J. of Heat and Fluid Flow*, **27**(4), 585–593, (2006).
4. Klein, M., Sadiki, A., and Janicka, J.: A digital filter based generation of inflow data for spatially developing direct numerical or large eddy simulations, *J. of Comp. Physics*, **186**(2), 652–665, (2003).
5. Lee, S., Lele, S. K. and Moin P.: Simulation of spatially evolving turbulence and the applicability of Taylor's hypothesis in compressible flow. *Physics of Fluids A: Fluid Dyn.*, **4**(7), 1521–1530 (1992).
6. Nicoud, F. and Ducros, F.: Subgrid-scale stress modelling based on the square of the velocity gradient tensor, *Flow Turbul. Combus.*, **62**(3), 183–200 (1999).
7. Matha, M., Morsbach, C., and Bergmann, M.: A comparison of methods for introducing synthetic turbulence, *7th Eur. Conf. on Comp. Fluid Dyn.*, (2018).
8. Morsbach, C., Franke, M.: Analysis of a synthetic turbulence generation method for periodic configurations, *Proceedings ERCOFTAC Direct and Large Eddy Simulations XI*, 61–67 (2017).
9. Michálek, J., Monaldi, M., and Arts, T.: Aerodynamic performance of a very high lift low pressure turbine airfoil (T106C) at low *Reynolds* and high *Mach* number with effect of free stream turbulence intensity, *J. of Turbomach.*, **134**, (2012).
10. Poinsot, T., and Lele, S. K.: Boundary conditions for direct simulations of compressible viscous flows, *J. of Computational Physics*, **101**, 104–129 (1992).
11. Sandhu, H. and Sandham, N.: Boundary conditions for spatially growing compressible shear layers, *Tech. Rep. QMW-EP-1100, QM & Westfield College*, (1994).
12. Roach, P. E.: The generation of nearly isotropic turbulence by means of grids, *Int. J. of Heat and Fluid Flow*, **7**(2), 117–125 (1986).
13. Schlüß, D., Frey, C. and Ashcroft, G.: Consistent non-reflecting boundary conditions for both steady and unsteady flow simulations in Turbomach. a plications *ECCOMAS Congress 2016*, (2016).
14. Smagorinsky, J.: General Circulation Experiments with the Primitive Equations, *Monthly Weather Review*, **3**(91), 99–164 (1963).
15. Shur, M. L., Spalart, P. R., Strelets, M. K., and Travin, A. K.: Synthetic turbulence generators for RANS-LES interfaces in zonal simulations of aerodynamic and aeroacoustic problems. *Flow Turbul. Combus.*, **93**(1), 63–92 (2014).
16. Thompson, K. W.: Time dependent boundary conditions for hyperbolic systems, *J. of Comp. Physics*, **68**(1), 1–24 (1987).
17. Wilcox, D. C.: Reassessment of the scale-determining equation for advanced turbulence models, *AIAA J.*, **26**(11), 1299–1310 (1988).